Journal of Neuroscience Methods 378 (2022) 109660

Contents lists available at ScienceDirect

Journal of Neuroscience Methods

journal homepage: www.elsevier.com/locate/jneumeth

Short communication

Detecting slow narrowband modulation in EEG signals

Maren E. Loe [a], Michael J. Morrissey [c], Stuart R. Tomko [b], Réjean M. Guerriero [b], ShiNung Ching [a,*]

[a] Department of Electrical and Systems Engineering, Washington University in St. Louis, 1 Brookings Drive, St. Louis 63130, MO, USA
[b] Division of Pediatric Neurology, Department of Neurology, Washington University School of Medicine, 660 S. Euclid Ave, St. Louis 63110, MO, USA
[c] St. Louis Children's Hospital, One Children's Place, St. Louis 63110, MO, USA

ARTICLE INFO

Keywords:
EEG modulation
Slow oscillations
2000 MSC:
92CXX
92C55
PACS:
87.19
87.85
43.60

ABSTRACT

Background: We observed an unusual modulatory phenomenon in the electroencephalogram (EEG) of pediatric patients with acquired brain injury. The modulation is orders of magnitude slower than the fast EEG background activity, necessitating new analysis procedures to systematically detect and quantify the phenomenon.
New method: We propose a method for analyzing spatial and temporal relationships associated with slow, narrowband modulation of EEG. We extract envelope signals from physiological frequency bands of EEG. Then, we construct a sparse representation of the spectral content of the envelope signal across sliding windows. For the latter, we use an augmented LASSO regression to incorporate spatial and temporal filtering into the solution. The method can be applied to windows of variable length, depending on the desired frequency resolution.
Results: The sparse estimates of the envelope power spectra enable the detection of narrowband modulation in the millihertz frequency range. Subsequently, we are able to assess non-stationarity in the frequency and spatial relationships across channels. The method can be paired with unsupervised anomaly detection to identify windows with significant modulation. We validated such findings by applying our method to a control set of EEGs.
Comparison with existing methods: To our knowledge, no methods have been previously proposed to quantify second order modulation at such disparate time-scales.
Conclusions: We provide a general EEG analysis framework capable of detecting signal content below 0.1 Hz, which is especially germane to clinical recordings that may contain multiple hours worth of continuous data.

1. Introduction

Electroencephalography (EEG) is commonly used for clinically monitoring neurological status of critical care patients Herman et al. (2015). In this context, EEG interpretation is often performed by means of visual examination of waveforms, which requires specialized training. Increasingly, this practice is being paired with quantitative analyses using statistical signal processing to summarize hours long recordings into more interpretable time-varying parameters or summary measures, which often include analyses in the frequency domain O'Toole and Boylan (2019); Foreman and Claassen (2012). The premise is that such approaches can provide more objective and accessible biomarkers and insights regarding the neurological status of patients.

1.1. Modulatory phenomena in EEG

Decomposing EEG signals in terms of their frequency components, i.e., power spectral analysis, is a practice that goes back many decades Nuwer (1988). One area of more recent focus within the area of spectral analysis has been in capturing structured interactions between power at two or more frequencies. The goal of such analyses is to identify situations in which power within one frequency range or band may be evolving with respect to time in a manner that is systematically related to the power within some other, distinct, frequency range. A canonical example of such frequency-frequency interaction occurs when one component of the signal modulates another. Phase-amplitude and phase-phase coupling are examples of such interaction, and a variety of techniques have been developed to resolve such phenomena in EEG signals Dvorak and Fenton (2014); Kovach et al. (2018); Tort et al.

Abbreviations: EEG, Electroencephalogram; PAC, Phase-amplitude coupling.

* Corresponding author.
E-mail address: shinung@wustl.edu (S. Ching).

https://doi.org/10.1016/j.jneumeth.2022.109660
Received 10 February 2022; Received in revised form 8 June 2022; Accepted 25 June 2022
Available online 30 June 2022

(2008); Jensen and Colgin (2007). These techniques generally involve a two-step process: (i) a step to extract frequency components of interest, e.g., by means of filtering, and (ii) a step to relate the extracted components, e.g., their alignment over time, either in terms of phase or power.

In traditional power spectral analysis, the types of frequency bands present in the signal may be quite variable depending on the context. Different types of brain injuries, disorders, and cognitive functions have been associated with quite distinct spectral features Foreman and Claassen (2012); Aydín (2009). Power can also vary widely across individuals. Similarly, modulatory phenomena in the EEG can be highly diverse, with different frequencies being involved and implicated with various aspects of brain function Jensen and Colgin (2007); Van Zaen et al. (2010); Zandvoort and Nolte (2021). It remains unclear whether these phenomena are mechanistically related at the level of their underlying neural circuit dynamics.

1.2. Slow modulation in clinical EEG

Much of the recent emphasis in modulatory EEG dynamics has focused on interaction between signal components that are commensurate in their frequencies, i.e., within the canonical EEG frequency bands spanning 0.5–50 Hz Tort et al. (2008). Recently, our group described a very slow (< 0.01 Hz) modulation that appears in the EEG of pediatric patients with newly acquired brain injuries Guerriero et al. (2021); Loe et al. (2022). This phenomenon lasts for tens of minutes, during which EEG power waxes and wanes with periodicity on the order of minutes (see Fig. 1A for a representative example in the time domain). Within each cycle, the EEG can retain a banded power spectral density reflective of more traditional oscillatory brain activity. We previously referred to this phenomenon as a macroperiodic oscillation, insofar as the modulation occurs at an 'outer' level of description relative to fast EEG activity. In prior work, we applied a preliminary form of a novel method for comparing said modulation across patients Loe et al. (2022). The overall goal of this paper is to describe an EEG analysis method to systematically characterize very slow modulation of this sort and track the dominant frequency of modulation across time and space.

1.3. Overview of methodological challenges and strategy

The principal challenge associated with detecting slow modulation is the low frequency range involved. At a pragmatic level, designing filters to extract activity < 0.01 Hz is difficult and computationally arduous. At a more fundamental level, it is unclear how much would be gained by such extraction, given the modulatory nature of the phenomenon. Consider, for example, the elementary example of a signal $y(t) = \sin(f_1 t)\sin(f_2 t)$, which is linearly composed of tones at $f_1 - f_2$ and $f_1 + f_2$. If f_1 and f_2 are orders of magnitude separated, then it may be of limited theoretical value to filter for the slower frequency.

Furthermore, the modulation itself may be nonstationary, bringing into consideration time-frequency resolution tradeoffs in any potential analysis approach, and traditional analysis of frequency-frequency interactions in EEG require *a priori* selection of frequency bands Dvorak and Fenton (2014); Kovach et al. (2018); Tort et al. (2008); Jensen and Colgin (2007), which may limit its use as a discovery tool for novel interactions or interactions across disparate timescales. Recent work has begun to address the former issue Munia and Aviyente (2022); Bertrand et al. (2020), but these approaches have not been adapted to track interactions at disparate time-scales. To engage with these challenges, we propose an EEG analysis method to quantify slow modulation. The proposed method integrates two levels of time-frequency analysis. The first level involves the extraction of the signal power envelope within particular frequency ranges of interest. The second level consists of finding a sparse spectral representation of the obtained envelope within a sinusoidal basis. This second step builds, in essence, a regularized spectral representation aimed at detecting narrowband structure (i.e., sinusoidal modulation) within the power envelope. The primary contribution of this paper is to formally outline this procedure and demonstrate its capabilities and efficacy within a particular context of use in the neurocritical care setting, the identification of aberrant modulation in EEG recordings of children with brain injury.

2. Materials and methods

2.1. Patient data and preprocessing

To provide proof of concept demonstrations of the proposed method, we used 10 exemplar subjects from the dataset described in Guerriero et al. (2021); Loe et al. (2022), where the macroperiodic oscillation phenomenon was described. These patients were monitored in the cardiac, neonatal, and pediatric intensive care units (CICU, NICU, and PICU) at St. Louis Children's Hospital (St. Louis, MO, USA) between September 2016 and May 2019, aged 0–2.5 years at admission. For each patient, we analyzed 12 h of 21-channel (10−20) 200 Hz EEG (Nihon Koden).

We identified an additional 5 patients who had EEG monitoring in the CICU, NICU, or PICU, but for whom there was no visually appreciable oscillatory modulation in the frequency domain of the EEG. The second cohort was used as a control group in the validation of our methods.

Clinical characteristics of the clinical populations are described in Loe et al. (2022). This study was approved by the Institutional Review Board (IRB) at Washington University in St. Louis.

All data were analyzed in MATLAB (Mathworks, Natick, MA, USA). EEG data was bipolar montaged (LB-18.1) Acharya et al. (2016); we then obtained multi-taper spectrograms (30 s windows, 6 s step). We calculated the envelope signal at the physiologically informative frequency bands: 0.5–3 Hz, 3–8 Hz, 8–15 Hz, and 15–30 Hz O'Toole and Boylan (2019). The envelope signals were filtered via moving average of one minute to obtain a smoothed envelope signal, upon which the proposed method was then applied.

3. Theory and calculations

3.1. Sparse spectral estimates of power envelopes

Our preliminary findings in Guerriero et al. (2021) relied on visual identification of modulation in the frequency domain of EEG recordings. To formally extract this modulation, we propose a multi-step analysis procedure as follows:

3.1.1. Envelope extraction

The first level of analysis involves extracting the power envelope within frequency bands of interest. There are a variety of established methods for such extraction, including the use of filtering followed by application of Hilbert transforms Dvorak and Fenton (2014). In our proposed procedure, we first estimate a time-frequency spectrogram of the raw signal in channel k, denoted $S_k(f, t)$, where $t = 1, 2, 3\ldots$ index successive temporal windows. We obtain a band-limited spectral envelope as:

$$\overline{S}_{k,\rho}(t) = \sum_{f \in F_\rho} \frac{1}{|F_\rho|} S_k(f, t), \tag{1}$$

where F_ρ is a set of frequency components (nominally constituting a contiguous band). The above is then windowed for subsequent analysis, i.e., the i^{th} window of the spectral envelope is given by:

$$\Gamma_{k,\rho}(i) = \left[\overline{S}_{k,\rho}(iT_m) \quad \overline{S}_{k,\rho}(iT_m + 1) \quad \ldots \quad \overline{S}_{k,\rho}(iT_m + N_m)\right], \tag{2}$$

where $T_m, N_m \in \mathbb{Z}^+$ are tunable parameters governing the window step size and length, respectively.

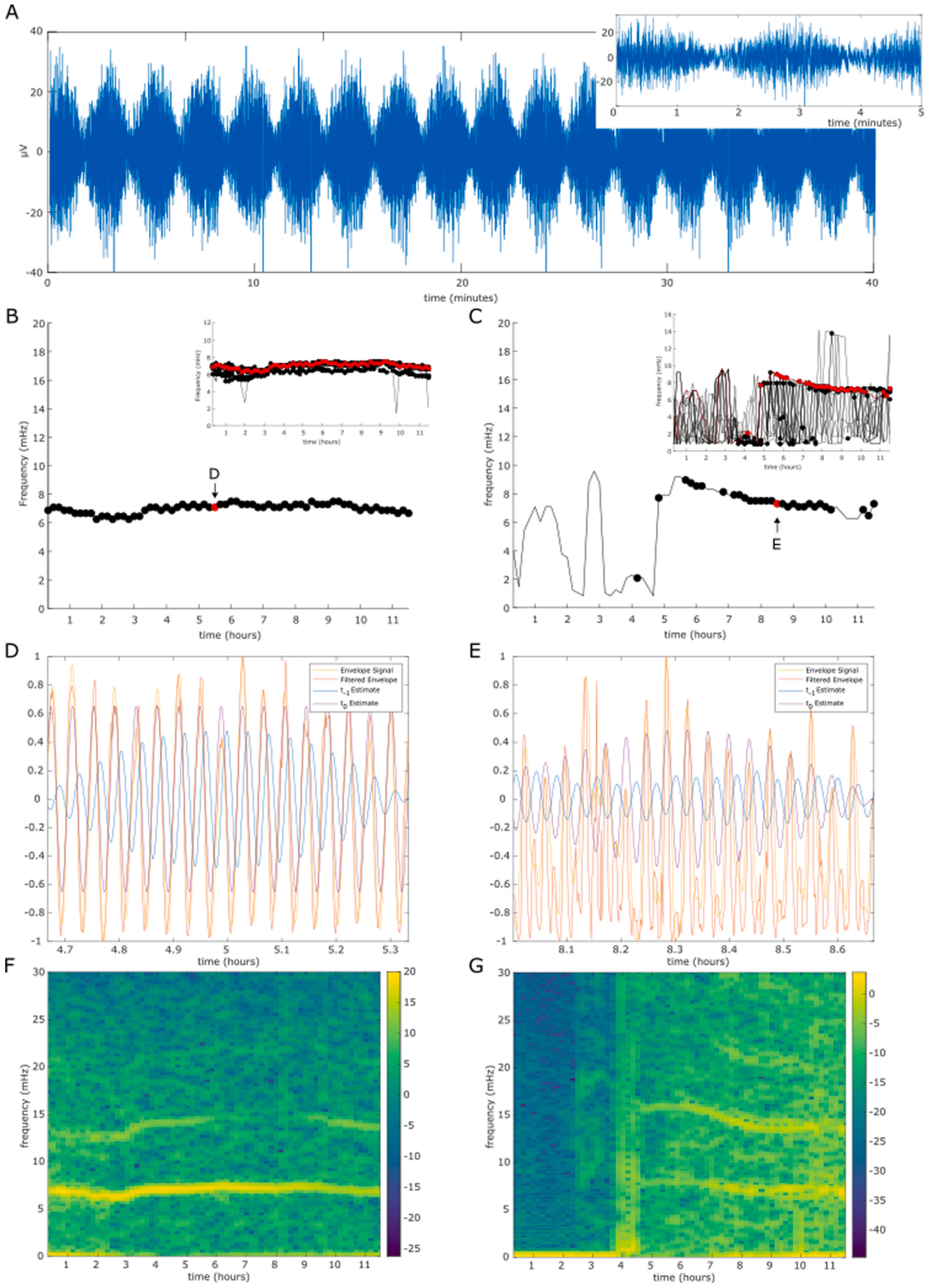

Fig. 1. Dominant frequency tracking: A) bandpass-filtered EEG from one patient (same patient depicted in B, D, F) depicting EEG across 40 min; inset: 5 min of bandpass-filtered EEG. B, C) dominant frequency across 12 h, in one channel for two patients, with overlay of the dominant frequencies in all channels inset. D, E) envelope signal comparison, depicting the envelope signal, filtered envelope signal, estimated envelope signal (t_0), the spatially weighted prior estimate from t_{-1}. F, G) Spectrograms of the full envelope signal across 12 h, with high power in narrow bands at the same frequencies identified in dominant frequency tracking.

3.1.2. Sparse spectral estimates of envelope signals

The remainder of the process focuses on analysis of $\Gamma_{k,\rho}(i)$, in order to understand any harmonic structure (i.e., modulation) that may be present. In our clinical data, we can clearly see such structure in a second time-frequency spectrogram applied to $\Gamma_{k,\rho}(i)$ (see, e.g., Fig. 1F, G). Given the narrowband characteristics, we sought to adapt sparse estimation methods to quantify this structure.

We construct a sparse representation of the power spectral density of the second-level spectrogram in channel k, as follows:

$$\beta_{k,\rho}(i) = argmin_b \parallel \Gamma_{k,\rho}(i) - Xb\|_2^2 + \lambda_1 \parallel b\|_1, \tag{3}$$

Here, X is a dictionary of sinusoidal basis functions (i.e., an inverse Discrete Fourier Transform matrix). Thus, the coefficients $\beta_{k,\rho}(i)$ provide a sparse, Fourier-based decomposition of the envelope signal. This overall problem is sometimes referred to in the literature as basis pursuit denoising Bertrand et al. (2020), and can be solved by means of LASSO regression Tibshirani (1996).

3.1.3. Spatiotemporal filtering

Because we assume that modulation changes slowly across space and time, we add a spatiotemporal regularizer to the basic formulation, resulting in

$$\beta_{k,\rho}(i) = \text{argmin}_b \parallel \Gamma_{k,\rho}(i) - Xb\|_2^2 + \lambda_1 \parallel b\|_1 + \lambda_2 \parallel b - \overline{\beta}_{k,\rho}(i-1)\|_2^2, \tag{4}$$

with

$$\overline{\beta}_{k,\rho}(i-1) = \sum_{l \in C_k} c_{l,k}\beta_{l,\rho}(i-1) \tag{5}$$

where C_k are the set of channels neighboring (in physical space) channel k, $c_{l,k}$ is the weight given to channel l relative to channel k, and $\beta_{l,i-1}$ is the sparse spectral estimate for that channel in the previous window.

3.2. Formulation of a modulation index

We seek to quantify the goodness of fit and sparsity of the estimate with a scalar value for each channel and window. To formulate an index, we compute two intermediate quantities. We first obtain the Pearson correlation between the estimate, $X\beta$, and the envelope signal, Γ,

$$r_{k,\rho}(i) = \frac{cov(\Gamma_{k,\rho}(i), X\beta_{k,\rho}(i))}{\sigma_{\Gamma_{k,\rho}(i)}\sigma_{X\beta_{k,\rho}(i)}}. \tag{6}$$

We also compute a pseudo-entropy of the sparse spectral estimate $\beta_{k,\rho}$ as

$$h_{k,\rho}(i) = -\frac{1}{\log(\|\beta_{k,\rho}(i)\|_1)} \sum_j \frac{\omega_{j,i}}{\|\beta_{k,\rho}(i)\|_1} \log\left(\frac{\omega_{j,i}}{\|\beta_{k,\rho}(i)\|_1}\right), \tag{7}$$

where

$$\omega_{j,i} = \left|(\beta_{k,\rho}(i))_j\right| \tag{8}$$

i.e., the magnitude of the j^{th} coefficient of $\beta_{k,\rho}(i)$, which corresponds to the power at the j^{th} frequency component embedded in X. If the solution $\beta_{k,\rho}(i)$ was sparse, i.e., if the elements are mostly zero with few non-zero elements, then $h_{k,\rho}(i) \approx 0$. Then, we formulate a modulation index, denoted q:

$$q_{k,\rho}(i) = r_{k,\rho}(i)(1 - h_{k,\rho}(i)) \tag{9}$$

Since r, $h \in [0,1]$, we have $q \in [0,1]$, with high values of q occurring when the signal presents strong sinusoidal narrowband modulation (i.e., when reconstruction is accurate using a very small number of spectral components). Similarly, low values of q indicate no narrowband modulation.

3.3. LASSO regression

Concretely, we solve (4) via the prototypical LASSO regression

$$\begin{aligned} \beta_{k,\rho}(i) \quad &= \text{argmin}_b \parallel \widehat{\Gamma}_{k,\rho}(i) - \widehat{X}\beta_{k,i}\|_2^2 + \lambda_1 \parallel \beta_{k,i}\|_1 \\ \text{where} \quad \widehat{\Gamma}_{k,\rho}(i) &= \begin{bmatrix} \Gamma_{k,\rho}(i) \\ \lambda_2 \overline{\beta}_{k,\rho}(i-1) \end{bmatrix}, \text{ and } \widehat{X} = \begin{bmatrix} X \\ \lambda_2 I \end{bmatrix}, \end{aligned} \tag{10}$$

where we perform the regression in a sliding window manner (i.e., indexed by i). For each patient and frequency band F_ρ, and for each window i we obtained the quantitative solution for parameters λ_1 and λ_2 that maximized $q_{k,\rho}(i)$. The regression was solved in MATLAB, which uses simultaneous coordinate descent to obtain LASSO solutions for $\lambda_1 \in [0, \lambda_{\max}]$, where $\lambda_{\max}$ is the parameter which imposes a solution with one nonzero component Friedman et al. (2010). This was done iteratively with $\lambda_2 = \{0, 0.01, 0.02, 0.04, 0.08, 0.16\}$. This results in a tensor $Q \in \mathbb{R}^{T \times K \times N}$ such that $q_{k,\rho}(i) \equiv q_{i,k,\rho} \in Q$ was the q value at the time window i, for channel k, in the frequency band ρ.

3.4. Bootstrapping and unsupervised anomaly detection

The above method can be paired with an unsupervised anomaly detection process via bootstrapping to identify significant q values. For this purpose, we generate surrogate noise data for each EEG signal. The surrogate noise data was obtained by generating time series data with the same pair-wise frequency content (amplitudes) as the bipolar-montaged EEG data. We then subjected this surrogate data to the same modulation analysis method as the true envelope signal, resulting in a surrogate tensor $\widehat{Q}$ of the same dimension as the true Q.

For each frequency band F_ρ and channel k, we generated an empirical distribution of q values over the k, ρ dimension of $\widehat{Q}$. We calculated the channel-wise mean, $\mu_{k,\rho}$, and standard deviation, $\sigma_{k,\rho}$ of this surrogate distribution. From these values, we generated a normal distribution, $\sim \mathcal{N}(\mu_{k,\rho}, \sigma_{k,\rho})$, against which we tested the statistical significance of $q_{i,k,\rho}$. Significant modulation of the envelope signal was defined by time windows with $p < 0.01$.

3.5. Dominant frequency tracking

To track the dominant frequencies of modulation across time, we obtained the dominant frequency, $f_{k,\rho}(i)$, as the frequency component with the highest weight $\omega_{j,i}$ in (8).

3.6. Spatial Correlations

To quantify spatial manifestation of modulation, we generated a reconstructed envelope signal at each time window:

$$\widehat{S}_{k,\rho}(i) = X\beta_{k,\rho}(i), \tag{11}$$

where $\beta_{k,\rho}(i)$ is the solution to the LASSO regression for frequency band F_ρ, in channel k, at the i^{th} window. Because not all channels had the same dominant frequency for each time, we quantified spatial lag by calculating the cross-correlation of the envelope estimates between the dominant channel and all other channels:

$$m^*_{k,\rho}(i) = \max_{m=0,1,\ldots,N/} 2\widehat{R}_{\widehat{S}_{k,\rho}(i),\widehat{S}_{l,\rho}(i)} \tag{12}$$

Where $\widehat{S}_{k,\rho}(i)$ is the reconstructed envelope signal of frequency band ρ, for the i^{th} time window of the k^{th} channel, for all channels $l \ddagger k$. The lag time, $t^*_{k,\rho}(i) = \frac{m^*_{k,\rho}(i)}{f_s}$, between channels was determined by f_s, the sampling frequency, and m^*, the offset at the maximum cross-correlation value for each channel, k, in relation to the dominant channel, l, for each frequency band F_ρ.

4. Results

We applied the proposed methodology to long epochs of EEG data from 10 patients from Guerriero et al. (2021); Loe et al. (2022) and 5 patients without any visually aberrant activity in the frequency domain as clinically adjudicated.

We computed $S_{k,t}(f)$ using standard multi-taper power spectral methods with $T_w = 30s$ with 6s step (i.e., 24s overlap), resulting in an effective sampling rate of $\Gamma_{k,\rho}(i)$ of $f_s = 1/6$ Hz. For envelope analysis we used a window of $N_m = 400$ (i.e., 40 min) advanced in $T_m = 100$ (10 min) steps. Our dictionary of sinusoids, $X \in \mathbb{R}^{n\times m}$, spanned a range of frequencies, from $f_{min} = \frac{2f_s}{N_m}$, to $f_{max} = \frac{f_s}{4}$. We included harmonic components every $\frac{f_{min}}{4}$Hz (resulting, in our example, in the evaluation of frequencies 0.8− 41.7mHz).

4.1. Detecting and tracking dominant modulation frequency

For each of the 10 patients, we obtained Q_ρ for four bands: $F_1 \in (0.5Hz, 3Hz)$, $F_2 \in (3Hz, 8Hz)$, $F_3 \in (8Hz, 15Hz)$, $F_4 \in (15Hz, 30Hz)$. The method indicated that each of the 10 patients had at least one channel with 2 h of significant narrowband modulation over all F_ρ. The means of significant value entries in Q_ρ were between 0.59 and 0.73. The dominant modulation frequency for two separate patients is depicted in Fig. 1B and C. The method successfully identifies the dominant frequency of the envelope signal, and our q index quantified both sparseness and goodness of fit of the LASSO solution. For Fig. 1D and E, the q value in the window depicted was 0.96 and 0.68, respectively. Furthermore, the dominant frequencies identified by our algorithm (Fig. 1B and C) matched the visually evident narrowband power in the corresponding spectrogram of the envelope signal in Figs. 1F and G.

4.1.1. Adjusting window length for lower frequencies

For four of the 10 patients, the dominant modulation frequency was one of the four lowest frequencies in the frequency dictionary, X, ($f = \{\frac{2f_s}{N_m}, \frac{5f_s}{2N_m}, \frac{3f_s}{N_m}, \frac{7f_s}{2N_m}\}$), during at least half of the significant windows. This suggests that the true dominant frequency, if significant, is lower than the resolution afforded by the analysis window N_m. In these cases, the method affords the flexibility to re-analyze with longer windows. In our example, we re-analyzed these four patients with an 80 min window and 20 min time step. The secondary analysis confirmed that a substantial proportion of the low dominant frequency values obtained on the first analysis were indeed correct and significant for three of the four patients. For the fourth patient, a majority of the significant values fell below the frequency threshold of the secondary analysis. However, the small number of remaining windows with significant strong modulation were temporally continuous, suggesting true slow modulation, albeit for a shorter duration. The mean of the entries in the Q_ρ of significant windows after the secondary analysis was within 0.01 of those from the initial analysis.

4.2. Spatial relationships

Using the envelope estimate, $\widehat{S}_{k,\rho}(i) = X\beta_{k,\rho}(i)$ from the sparse solution vectors from 10, we characterized the extent to which modulation was synchronous across space. In this regard, the method allows us to observe both spatially widespread modulation (e.g. Fig 2A, C) and spatially constrained hemispheric modulation (Fig 2B, E). Non-zero lag times were occasionally obtained but were typically the result of dominant frequency mismatch, rather than a out-of-phase modulation (Fig 2D, F).

4.3. Assessment of modulation in controls

We also applied our methods to 5 pediatric patients whose EEG did not have aberrant activity in the frequency domain, based on clinical EEG assessments. Fig. 2G compares the proportion of windows with significant modulation, and the distribution of modulation index values from these patients to the 10 high suspicion patients used previously (here, $T_m = 100$, $N_m = 400$). Overall the controls have lower average q of significant windows (highest control $q = 0.59$, lowest patient $q = 0.60$), and a lower proportion of significant windows (highest for control 12.7%, lowest for patient 13.4%). There are two interpretations of this outcome. First, the method confirms the initial clinical adjudication based on visual inspection, differentiating these records from the patient cohort. On the other hand, the method suggests that some slow dynamics may nonetheless be present in these recordings, perhaps at a level that is not visually apparent but nonetheless quantitatively significant, albeit with less spatial and temporal continuity.

5. Discussion

We describe a systematic procedure for identifying second order modulation in electrophysiological recordings. Notably, the method is capable of identifying modulation in the millihertz range, much slower than has been treated by prior second-order analysis methods. We have incorporated the spatial and temporal information intrinsic to EEG (i.e. channel locations) into our time-windowed frequency-tracking method, and we exploit the imposed sparsity of our solution to generate a univariate index value.

5.1. Detecting oscillatory modulation

Our method expands on prior methods for detecting second order modulation, like the bispectrum Kovach et al. (2018), cross-frequency coupling Tort et al. (2008), and Morlet wavelet analyses min An et al. (2021), all used to quantify phase-amplitude coupling (PAC) between common frequency bands, e.g. theta-gamma coupling. Specifically, we are able to address gaps in other methods by quantifying the relationship between harmonic signal components at frequencies differing by orders magnitude. Traditional methods of detecting second order modulation require bandpass filtering; the slow frequencies tracked by our method would require longer EEG recording epochs to apply computationally intensive filters, and resulting in lower temporal resolution. The modulatory phenomenon visually identified in Guerriero et al. (2021); Loe et al. (2022) and further quantified using our proposed method differs from previously described PAC in the frequencies implicated and the highly disparate time-scale separation. As described in our prior works, while such a slow phenomenon could be associated with artifact, patients exhibited temporal heterogeneity (both within and across patients), the dominant frequencies were identified across a range (2–12mHz), recordings exhibited a range in q values, and EEG was obtained from multiple ICUs across 3 years. In one cohort, strength of modulation correlated with outcomes Loe et al. (2022). Additionally, one patient described in that paper had concurrent intracranial pressure and heart rate date recorded by a separate device, which demonstrated significant modulation at the same frequency of EEG modulation. As such, the underlying physiological mechanisms generating the millihertz frequencies depicted in Fig. 1 likely differ from traditional PAC, which highlights the utility of our method to establish novel phenomena and support their further study.

5.2. Advantages

We implemented this method without *a priori* knowledge of the frequencies of interest, highlighting its potential utility as a discovery tool or for real-time patient monitoring; our subsequent re-application of the method to longer time windows verified the validity of the dominance of low modulatory frequencies and further demonstrates the value in this type of method. Our method incorporates modifications of basis pursuit denoising-dynamic filtering (BPDN-DF) Bertrand et al. (2020)

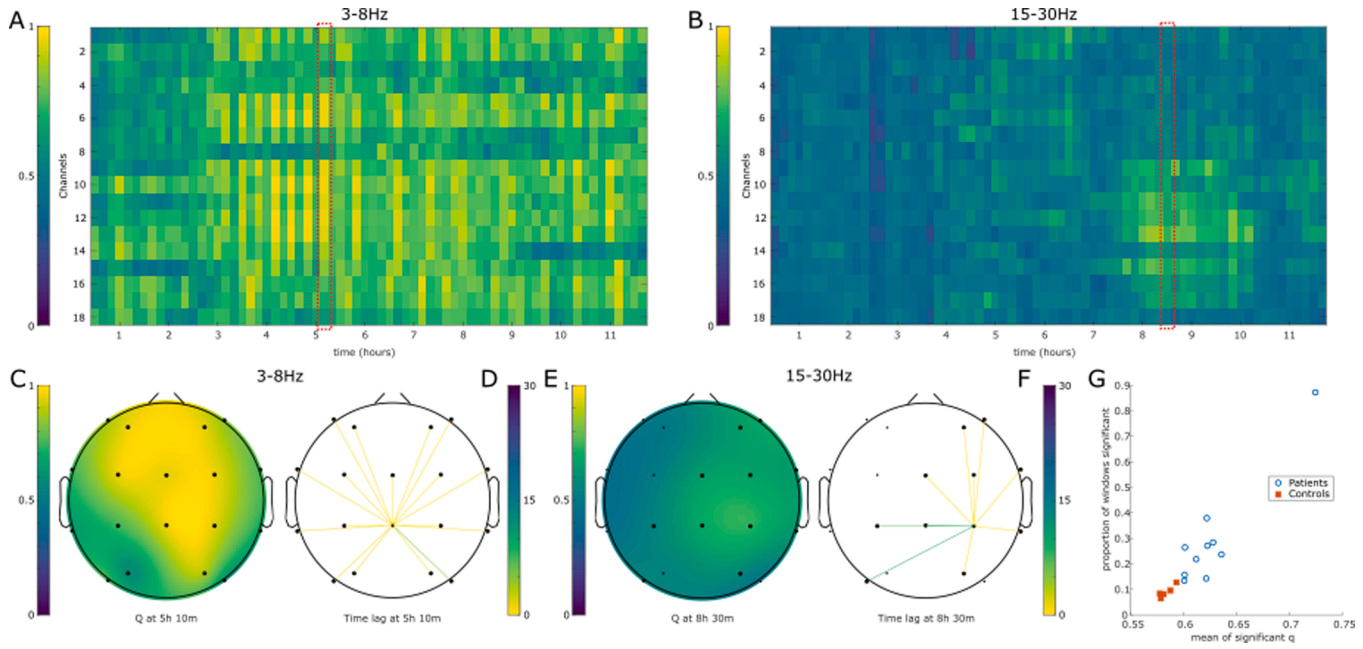

Fig. 2. Spatial manifestation of modulation. A) Heatmap of q values for all channels across 12 h, demonstrating spatially widespread, persistent modulation. The average q value for significant time windows was 0.73 for this frequency band. B) Heatmap of q values for all channels across 12 h, demonstrating hemispheric manifestation of hours-long modulation. The mean q value of significant time windows for this frequency band was 0.62. C) Spatially widespread, strong, significant modulation depicted across all 18 channels. D) Lag times between all significant channels and the dominant channel, broadly synchronous. E) Right hemisphere dominant modulation, with some significant modulation in the left hemisphere. F) Lag times between significant channels and the dominant channel, suggesting some lag across hemispheres, attributed to different dominant frequencies. G) Comparison of mean significant q values and proportion of total windows deemed significant in patients and controls, across all frequency bands F_ρ.

and matching-pursuit dynamic phase-amplitude coupling (MP-dPAC) Munia and Aviyente (2022) into a distinct workflow. Importantly, one of the primary goals of our method is to detect very slow ($<$ 0.1 Hz) modulation of the EEG signal, and we established the feasibility of quantifying such slow modulation and tracking it across time. To the best of our knowledge, nobody else has applied similar techniques to track significant frequency-frequency interactions below 0.1 Hz, let alone on the order of mHz. The proposed method also easily pairs unsupervised anomaly detection to generate probabilistic thresholds for the significance of the index values, using surrogate noise signals. This substantiated our overall claims that slow modulation was present in the studied EEG signals, and that this modulation is detectable by the proposed method. Furthermore, we validated the method by demonstrating the absence of significant modulation in five control patients.

The primary objective of this manuscript was to describe novel methodology for detecting and tracking very slow modulation in the spectral domain; a secondary objective was to further demonstrate the utility of such methods in a small number of clinical patients and controls. While we applied our method very young pediatric patients and did not discuss physiological hypotheses for slow modulation (see Loe et al., 2022), this method is a tool for discovery of novel frequency-frequency interactions across disparate time-scales and further study should be done in a variety of clinical populations. In those populations, further validation would be necessary to characterize reliability and clinical significance (i.e., pathophysiology) in large cohorts.

6. Conclusion

In summary, we have proposed a method grounded is principled signal processing techniques for detecting very slow narrowband modulation in EEG signals. We demonstrated that our method can establish significance of modulation, track the dominant frequency of modulation over time, and provide insights into spatial and temporal relationships of modulation. The method may be germane to the assessment of clinical EEG involving hours of patient recordings.

Declarations of Interest

None.

Acknowledgements

This research was partially funded by the Washington University Institute of Clinical and Translational Sciences grant UL1TR002345 from the National Institutes of Health (NIH) and grant 1653589 from the National Science Foundation.

References

Acharya, J.N., Hani, A.J., Thirumala, P., Tsuchida, T.N., 2016. American clinical neurophysiology society guideline 3: a proposal for standard montages to be used in clinical EEG. Neurodiagnostic J. 56 (4), 253–260. https://doi.org/10.1080/21646821.2016.1245559.

Aydín, S., 2009. Comparison of power spectrum predictors in computing coherence functions for intracortical eeg signals. Ann. Biomed. Eng. 37 (1), 192–200.

Bertrand, N.P., Charles, A.S., Lee, J., Dunn, P.B., Rozell, C.J., 2020. Efficient tracking of sparse signals via an earth mover's distance dynamics regularizer. IEEE Signal Process. Lett. 27, 1120–1124. https://doi.org/10.1109/LSP.2020.3001760 arXiv:1806.04674.

Dvorak, D., Fenton, A.A., 2014. Toward a proper estimation of phase-amplitude coupling in neural oscillations. J. Neurosci. Methods 225, 42–56. https://doi.org/10.1016/j.jneumeth.2014.01.002 arXiv:NIHMS150003. ⟨http://www.ncbi.nlm.nih.gov/pubmed/24447842⟩.

Foreman, B., Claassen, J., 2012. Quantitative eeg for the detection of brain ischemia. Crit. Care 16. https://doi.org/10.1186/cc11230.

Friedman, J., Hastie, T., Tibshirani, R., 2010. Regularization paths for generalized linear models via coordinate descent. J. Stat. Softw. 33 (1), 1.

Guerriero, R.M., Morrissey, M.J., Loe, M.E., Reznikov, J., Binkley, M.M., Ganniger, A., Khanmohammadi, S., Guilliams, K.P., Ching, S., Tomko, S.R., 2021. Macroperiodic oscillations (MOs) are associated with seizures following acquired brain injury in young children. J. Clin. Neurophysiol. https://doi.org/10.1097/WNP.0000000000000828.

Herman, S.T., Abend, N.S., Bleck, T.P., Chapman, K.E., Drislane, F.W., Emerson, R.G., Gerard, E.E., Hahn, C.D., Husain, A.M., Kaplan, P.W., et al., 2015. Consensus statement on continuous eeg in critically ill adults and children, part i: indications. J. Clin. Neurophysiol.: Off. Publ. Am. Electroencephalogr. Soc. 32 (2), 87. https://doi.org/10.1097/WNP.0000000000000166.

Jensen, O., Colgin, L.L., 2007. Cross-frequency coupling between neuronal oscillations. Trends Cogn. Sci. 11 (7), 267–269. https://doi.org/10.1016/j.tics.2007.05.003.

Kovach, C.K., Oya, H., Kawasaki, H., 2018. The bispectrum and its relationship to phase-amplitude coupling. NeuroImage 173, 518–539. https://doi.org/10.1016/j.neuroimage.2018.02.033 arXiv:1705.10435.

Loe, M.E., Khanmohammadi, S., Morrissey, M.J., Landre, R., Tomko, S.R., Guerriero, R. M., Ching, S., 2022. Resolving and characterizing the incidence of millihertz eeg modulation in critically ill children. Clin. Neurophysiol. 137, 84–91.

min An, K., Ikeda, T., Hasegawa, C., Yoshimura, Y., Tanaka, S., Saito, D.N., Yaoi, K., Iwasaki, S., Hirosawa, T., Jensen, O., Kikuchi, M., 2021. Aberrant brain oscillatory coupling from the primary motor cortex in children with autism spectrum disorders. NeuroImage: Clin. 29 https://doi.org/10.1016/j.nicl.2021.102560.

Munia, T.T., Aviyente, S., 2022. Assessment of dynamic phase amplitude coupling using matching pursuit. J. Neurosci. Methods, 109610.

Nuwer, M.R., 1988. Quantitative EEG: I. techniques and problems of frequency analysis and topographic mapping. J. Clin. Neurophysiol. 5 (1), 1–44. https://doi.org/10.1097/00004691-198801000-00001.

O'Toole, J.M., Boylan, G.B., 2019. Quantitative preterm EEG analysis: the need for caution in using modern data science techniques. Front. Pediatr. 7 (174) https://doi.org/10.3389/fped.2019.00174.

Tibshirani, R., 1996. Regression shrinkage and selection via the lasso. J. R. Stat. Soc.: Ser. B (Methodol.) 58 (1), 267–288. https://doi.org/10.1111/j.2517-6161.1996.tb02080.x.

Tort, A.B., Kramer, M.A., Thorn, C., Gibson, D.J., Kubota, Y., Graybiel, A.M., Kopell, N.J., 2008. Dynamic cross-frequency couplings of local field potential oscillations in rat striatum and hippocampus during performance of a T-maze task. Proc. Natl. Acad. Sci. USA 105 (51), 20517–20522. https://doi.org/10.1073/pnas.0810524105. ⟨https://www.pnas.org/content/105/51/20517⟩.

Van Zaen, J., Uldry, L., Duchêne, C., Prudat, Y., Meuli, R.A., Murray, M.M., Vesin, J.M., 2010. Adaptive tracking of EEG oscillations. J. Neurosci. Methods 186 (1), 97–106. https://doi.org/10.1016/j.jneumeth.2009.10.018.

Zandvoort, C.S., Nolte, G., 2021. Defining the filter parameters for phase-amplitude coupling from a bispectral point of view. J. Neurosci. Methods 350, 109032. https://doi.org/10.1016/j.jneumeth.2020.109032.